Available online at www.sciencedirect.com
SCIENCE DIRECT®
Journal of Molecular Graphics and Modelling 22 (2004) 309–316
Journal of Molecular Graphics and Modelling
www.elsevier.com/locate/JMGM

The distribution of the unoccupied volume in glassy polymers

E. Schmidtke [a], K. Günther-Schade [a], D. Hofmann [b], F. Faupel [a,*]

[a] *Technische Fakultät der Christian-Albrechts-Universität zu Kiel, Lehrstuhl für Materialverbunde, Kaiserstrasse 2, D-24143 Kiel, Germany*
[b] *Institut für Chemie, GKSS Forschungszentrum GmbH, Kantstraße 55, D-14513 Teltow, Germany*

Received 11 March 2003; received in revised form 4 September 2003; accepted 10 November 2003

Abstract

The aim of this paper is to present an improved method to describe the unoccupied volume in glassy polymers. The method is able to treat atoms with non-spherical symmetry. The fineness of the raster points scanning the unit cell can be as small as 0.01 nm. This method was used to determine the unoccupied volume of molecular dynamic simulations of poly(amide imide) unit cells by probing it with a tracer atom. Since the reachable unoccupied volume strongly depends on the tracer radius, we used tracer radii between 0.03 and 0.17 nm. The poly(amide imide)s were used in the present work because they are well characterized, especially there already exist free volume data determined by positron lifetime experiments.
© 2003 Elsevier Inc. All rights reserved.

Keywords: Unoccupied volume; Glassy polymers; Hole sizes; Simulations; Positron annihilation lifetime spectroscopy (PALS)

1. Introduction

Positron annihilation lifetime spectroscopy (PALS) has been established in the last 15 years as a standard method to determine free volume hole sizes in polymers directly. The pick-off lifetimes of the $^3S_1$ state of positronium (*ortho*-positronium, termed *o*-Ps) which is a hydrogen atom-like state of a positron and an electron can be used as a probe for the hole sizes [1,2]. Since the beginning of the 1990s, average hole sizes are calculated from *o*-Ps lifetimes primarily based on the semi-empirical equation (Eq. (1)) of Jean [2]. This equation is based on a quantum mechanical approach of Tao [3] described for different potential wells and later modified by Eldrup et al. [4] for the temperature dependence of discrete lifetimes resulting in the prediction that positronium is annihilating in the larger free volume holes. This model is the so-called "standard model" where it is assumed that the Ps atom is confined to an infinitely deep spherical potential well.

$$\tau_{o\text{-Ps}} = \lambda_0^{-1}\left(1 - \frac{R_\mathrm{h}}{R_\mathrm{h}+\delta R} + \frac{1}{2\pi}\sin\left(\frac{2\pi R_\mathrm{h}}{R_\mathrm{h}+\delta R}\right)\right)^{-1} \quad (1)$$

The prefactor λ_0^{-1} is the reciprocal spin-averaged Ps annihilation rate of 0.5 ns [5]. The quantity R_h is the radius of the hole and the empirical parameter δR is the thickness of an electron layer describing the electron density of the surrounding molecules. The value of δR has been determined before to be 1.656 Å by fitting the equation to positron lifetime values measured in systems with holes of spherical symmetry and known hole sizes [2]. Although this approach is still discussed in the literature [6,7], it seems to be generally accepted [8].

Other authors also made quantum mechanical approaches to translate lifetimes to hole sizes but the potential forms are different from the step potential of Jean. Mukherjee et al. [9], for example, used the following expression:

$$U(r) = U_0 \tanh^2\left(\frac{r}{R_0}\right) \quad (2)$$

with R_0 as the radius of the detected spherical hole.

Another approach has been suggested by the same group [10] where the radial potential is approximated as follows:

$$U(r) = U_0\left(1 - \exp\left(\frac{r}{R_0}\right)\right) \quad (3)$$

The model parameters U_0 and R_0 also describe the potential depth, but they are different from Eq. (2).

All three approaches give comparable results for the translation of lifetimes to hole volumes.

In all cases, the basic model assumes a spherical hole within a homogeneous matrix. This approach is rather simple. The angle dependent part of the Schrödinger equation

* Corresponding author. Tel.: +49-431-8806225; fax: +49-431-8806229.
E-mail address: ff@tf.uni-kiel.de (F. Faupel).

1093-3263/$ – see front matter © 2003 Elsevier Inc. All rights reserved.
doi:10.1016/j.jmgm.2003.11.001

is separated, and only the radial part is left. These potentials do not take into account the real structure in the polymer but the remaining radial differential equation can be solved analytically. In all cases, the solution is only documented for the *s* ground state ($n = 1$). Activated states ($n > 1$) are not mentioned. So especially thermal activation is not taken into account.

One model which is able to take the thermal activation into account is published by Gidley et al. [11]. This model is also based on the potential wells of Tao and Eldrup, but a cuboid-type potential well is used. Its three dimensional Schrödinger equation separates in three one dimensional equations, which can be solved easily. All energy levels and eigenfunctions are known. Therefore, the temperature dependence can be taken into account in a simple way.

The problem is that all models assume only one type of hole symmetry and do not consider other shapes. In polymers, holes do not necessarily have spherical symmetry. Hence, significant changes of the positron lifetime parameters induced by deviations from the spherical symmetry are found [12,13]. Therefore, one important comment on the last international conference on positron annihilation [8,14] was that it is not useful just to apply a formula like Eq. (1). One should combine PALS measurements with simulations to understand what the positron really sees within the structure of the polymer. For this reason, it was necessary to undertake simulations on the one hand and to simultaneously examine the polymer structure as to how the positron interacts within the structure.

2. Geometrical approaches

There are several possibilities to describe the free volume. One is the unoccupied volume, which is defined as the difference between the molar volume of a substance and the volume occupied by the Van der Waals volume of the substance at a given temperature [15]. Older methods to calculate the space between the atoms are based on the approaches of Voronoi [16] and the triangulation of Delaunay [17]. The two dimensional principle of the “empty circuit” can be extended to three dimensions. The atom positions which are needed as vertices for this methods can be calculated by molecular dynamics or Monte Carlo simulations. In these simulations it can be seen that the “canonical polyhedron” originally established by Bernal [18] is not sufficient for fluids, polymers or amorphous metals because the assumption of similar atom distances to all neighbors is not fulfilled [20,21].

In the Delaunay triangulation, the position of the atoms is given by an irregular tetrahedron involving four atoms. In this case, only the position of the atom, not the shape or the size of the atoms are expressed. Since all atoms have the same size in the tetrahedron, this description is sufficient in monoatomic fluids or solids.

It is more difficult when the atoms are of different sizes, because the shells cover different volumes of the tetrahedrons and might overlap. Arizzi et al. [19] investigated polypropylene and polycarbonates with the Delaynay triangulation and considered the overlap of the Van der Waals spheres. In their article, the tetrahedra are combined to form holes in which a diffusor can move freely.

Further variants of the Voronoi diagram or the Delaynay triangulation can be found in the literature [22,23]. For the description of the hole size the tetrahedrons are joint together or a sphere is fitted in the tetrahedron.

All methods based on the Delaunay triangulation define atoms as spheres and do not consider the bonds and orientations in the molecules.

3. Model description

We want to present an improved way to describe the holes, which is able to take into account hole shapes without any limitations resulting from quantum mechanical models or spherical symmetry of the atoms in geometrical models. This model is able to yield the hole sizes, their distribution, shape, and compactness.

3.1. Definitions

The size of a hole depends strongly on the size of the probe which detects the hole. A large atom, for example, does not fit in every hole. The volume which is not occupied by the matrix atoms is usually defined as “unoccupied volume” [15]. The matrix atoms are assumed as hard spheres, however, our approach can also be applied for non-spherical symmetry. Matrix atoms are able to overlap, but a diffusor is not able to penetrate them. The probe which scans the hole has spherical symmetry and is called “tracer” in this context. Fig. 1 shows how a small tracer can pass a narrow connecting passage between two large holes and “sees” them as one. A large tracer detects them as two separate holes. In this figure, the squares connected by the tunnel are the border between matrix and hole. The white circles are the tracer spheres. The gray area is the detected hole. This phenomenon was already described by other authors [26]. But in this work we present results for the reachable hole sizes for different diffusor sizes. The gray area is the “reachable unoccupied volume”. We use this notation to distinguish this from the well defined “unoccupied volume”.

The detected holes are characterized by three parameters. The first parameter is the volume. The second parameter is the inertial tensor Θ, which gives a first indication about the shape of the hole. There are different methods to form scalars from the principal moments of inertia, M_1, M_2 and M_3, which can be the criteria for the shape. The third parameter is the compactness D. With the moments, $M_1 \geq M_2 \geq M_3$, the following parameters can be defined [24],

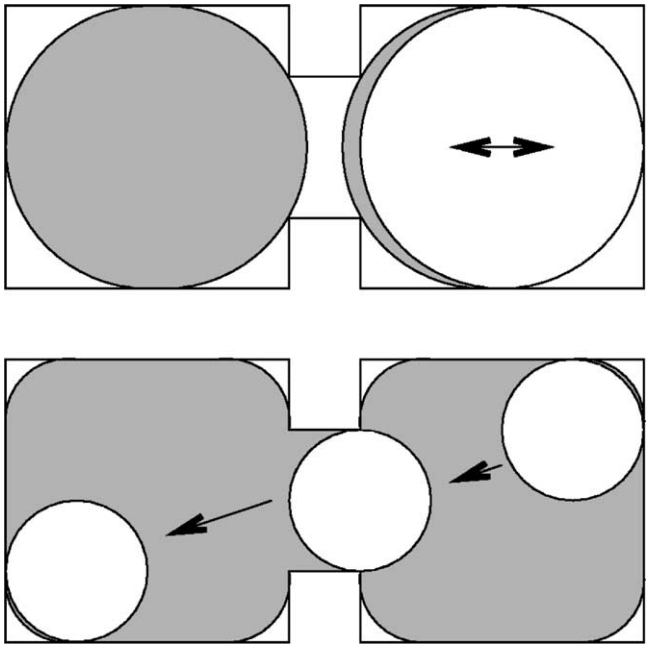

Fig. 1. Demonstration of the "reachable unoccupied volume". The squares connected by the tunnel are the border between matrix and hole. The white circles are the tracer spheres. The gray area is the detected hole. Shape and size of the hole are strongly dependent on the tracer radius. A small tracer can pass narrow connection passages between two large holes and "sees" them as one. A large tracer detects them as two separate holes.

which give the hole size and the deviation from the spherical symmetry:

- radius of inertia:

$$S^2 = M_1 + M_2 + M_3 \tag{4}$$

- deviation from spherical shape:

$$B = M_1 - \tfrac{1}{2}(M_2 + M_3) \tag{5}$$

- deviation from cylindrical shape:

$$C = M_2 - M_3 \tag{6}$$

Instead of a combination of these parameters, we used the half axes $a > b > c$ of the ellipsoid of inertia and the ratios $1 \geq b/a \geq c/a$ to characterize the hole shapes.

A new criterion to describe holes is the deviation from the generalized form of the ellipsoid of inertia. The ellipsoid of inertia has always a larger volume than the hole it describes. The ratio

$$D = \frac{V\,(\text{ellipsoid of inertia})}{V\,(\text{hole})} > 1 \tag{7}$$

is called compactness. The value $D = 1$ means, that the hole itself is an ellipsoid. A single massive cube has a value of

$$D\,(\text{cube}) = 1.049\ldots \tag{8}$$

If this cube is joint to other cubes on every six sides this body has a value of

$$D\,(7\,\text{cubes}) = 1.176\ldots \tag{9}$$

Table 1
Parameters of the simulated unit cells

	Edge length (nm)	N atoms
PAI 1	2.806	1922
PAI 2	2.809	1924
PAI 3	2.782	1922
PAI 4	3.353	3202

and is not called "compact" anymore. Hollow spheres with an outer radius r and an inner radius (εr) $\varepsilon < 1$ have a value of

$$D = \frac{(1 - \varepsilon^5)^{3/5}}{1 - \varepsilon^3} \tag{10}$$

3.2. Application/transposing

The simplest way to determine the reachable unoccupied volume is to determine first the occupied volume. We applied this method to MD simulations of poly(amid imide), PAI polymers [27]. The corresponding PALS measurements have been published elsewhere [28,29]. The MD simulations are performed in cube-shaped unit cells. The lengths of the edges are dependent on the simulation data and are ~3 nm with up to 3000 atoms in the simulation cell.

The algorithm for the creation and validation of the packing models shall now be described in more detail. The InsightII/Discover software of molecular simulations [30,31] was utilized for the amorphous packing model construction. The cvff forcefield [32,33] was applied. The calculations were performed on IBM RS 6000 and SGI Octane workstations.

Initial bulk polymer packing cells including inserted small molecules were created utilizing the amorphous cell module [34] of the InsightII/Discover software. There, the polymer chains were grown at 303 K under cubic periodic boundary conditions (cf. Ref. [34] for details). The volume of the basic cell was chosen in such a way that to avoid packing algorithm related catenations and spearing of aromatic units. The procedure started with a very low initial packing density (typically 0.1 g/cm^3). Four independent models were constructed in this way (cf. Tables 1 and 2).

All initial packing models were subjected to extensive equilibration procedures. For these and all the other simulations, the following general conditions were used:

Table 2
Radii of the Van der Waals spheres in the polymer structure taken from reference [40]

Element	Radius (nm)
H	0.120
C	0.170
N	0.155
O	0.150
F	0.147
Si	0.210

Table 3
Basic equilibration cycle for the PAI packing models

Stage of equilibration	Status of p and T	Scaling factor for conformation energy terms in the forcefield	Type of non-bonded interaction energy terms in the forcefield	Scaling factor for atomic radii in non-bonded interaction energy terms	Time step (fs)
1	*NVT*, 303 K	0.001	Repulsive 4th order	0.5	0.05
2	*NVT*, 303 K	0.1	Repulsive 4th order	0.5	0.05
3	*NVT*, 303 K	0.1	Repulsive 4th order	2/3	0.05
4	*NVT*, 303 K	0.1	Repulsive 4th order	1	0.05
5	*NVT*, 303 K	1	Repulsive 4th order	1	0.05
6	*NVT*, 303 K	1	6–9 potential + Coulomb	1	0.05
7	10000 bar, 303 K	1	6–9 potential + Coulomb	1	0.2
8	*NVT*, 600 K	1	6–9 potential + Coulomb	1	0.5
9	*NVT*, 303 K	1	6–9 potential + Coulomb	1	1
10	30000 bar, 303 K	1	6–9 potential + Coulomb	1	0.2
11	*NVT*, 600 K	1	6–9 potential + Coulomb	1	0.5
12	*NVT*, 303 K	1	6–9 potential + Coulomb	1	1
13	50000 bar, 303 K	1	6–9 potential + Coulomb	1	0.2
14	*NVT*, 600 K	1	6–9 potential + Coulomb	1	0.5
15	*NVT*, 303 K	1	6–9 potential + Coulomb	1	1

NVT = constant, particle number *N*, volume *V*, and temperature *T* conditions.

(a) Minimum image periodic boundary conditions to make the systems numerically tractable and to avoid artificial symmetry effects.
(b) Cut-off distance for all non-bond interactions of 1.35 nm with a smooth switching function being used for all interatomic distances between 1.2 and 1.35 nm.
(c) Simulation time step 1 fs.
(d) Berendsen method [35] of temperature- and pressure bath (for NPT-MD stages, i.e. MD under constant particle number *N*, pressure *P*, and temperature conditions) coupling with a coupling constant of 100 fs to stabilize the intended system temperature and pressure during MD runs.

Due to the already mentioned catenation and spearing problem, a quite extensive equilibration cycle was needed. There also the additional problem, that the respective packing models need to be slowly compressed from a density of about 0.1 g/cm^3 to the respective real density via NPT-MD runs, was to be addressed. Table 3 shows an equilibration sequence containing annealing stages that could be successfully applied to the initial packing models of PAI.

After an equilibration cycle according to Table 3, each packing model was subjected to a short NPT-MD simulation at $p = 1$ bar and $T = 303$ K. There it was checked whether the refined system would relax at the experimental or otherwise predicted density of the real polymer. After the first equilibration cycle, however, the simulated density at 1 bar is usually 10–20% lower than the respective experimental value. This indicates that there is still a certain degree of unrealistic tensions in the simulated packing model that needs further equilibration. This was performed via repeatedly applying the following procedure:

(1) NPT-MD compression run at (1–5) $\times$ 10^4 bar to bring the system density well above the measured target value;
(2) equilibration of the resulting structure according to Table 3;
(3) 1 bar NPT run at 303 K.

The procedure was repeated as often as was needed to arrive at a stable density of the respective polymer near the experimental data. After the application of these extensive equilibration procedures, all PAI packing models showed density values at 1 bar that were at maximum 2% lower than the respective experimental data. The quality of the obtained models was further checked by applying the Gusev–Suter method [36,37] for the prediction of constants of diffusion and solubilities of small gas molecules. The resulting data were compared with respective experimental results. The coincidence was quite satisfying as was published elsewhere [38].

The unit cells obtained in the just described way were scanned with single points. A raster size of 0.01 nm was enough to detect a sphere. Each raster point is characterized by a single byte that contains the distance between this point and the next occupied point measured in raster points. The area within the Van der Waals spheres of the polymer atoms is marked as unreachable (the byte is set to zero).

This method seems to be similar to the method of Voorintholt et al. [25], which was used by Müller-Plathe et al. to study diffusion in polymers [26], but our method involves some improvements. We use a different function to determine the distance between tracer and atoms and our atoms are not necessarily of sherical symmetry. Due to more powerful computers being used nowadays, we were able to increase the fineness of the rastering from 0.1 to 0.01 nm. We made additional experiments with a fineness of 0.001 nm, but as long as atoms and tracers are calculated as hard spheres, these runs give no additional information.

For all remaining raster points, the distance to the next unreachable raster point is calculated and rounded to multiples

of 0.01 nm (integer). So it is possible to use distances up to 2.54 nm in the described data format. All larger distances are calculated with the value 255 = 2.55 nm = infinity which was never observed in the present MD data.

Since we consider the distance to the unreachable raster point, we are able to calculate atom symmetries which are not of spherical symmetry such as between atoms for an example.

If the tracer is of spherical symmetry with a radius of n raster points it should fit in a hole with values $N \geq n$. One simply has to take all raster points with a value of $N \geq n$. These raster points do not describe the hole completely. They are only the part of the hole in which the center of the tracer can reside in. It is necessary to put a sphere with a radius n around the center. The sum of these spheres is the "detectable unoccupied volume".

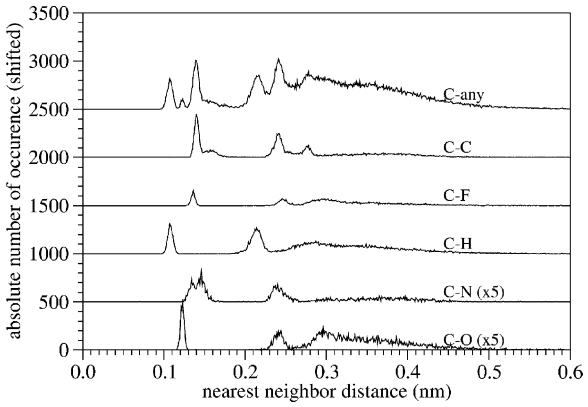

Fig. 4. The distances between the carbon atoms and their nearest neighbors. The upper curve is the sum of all distance distributions. The distributions related to the different partners are shown below.

4. Algorithm

We used the above described model to determine hole sizes in the polymer PAI(1) as a reference [27]. The structural formula is shown in Fig. 2. A two-dimensional cut through the unit cell is shown in Fig. 3. We had four different simulations of the cubical unit cell. The parameters are listed in Table 1.

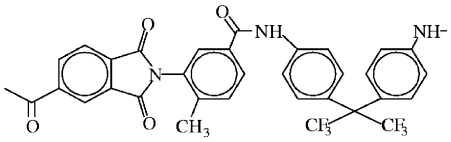

Fig. 2. The structural formula of the investigated PAI(1) poly(amid imid) membrane taken from reference [27].

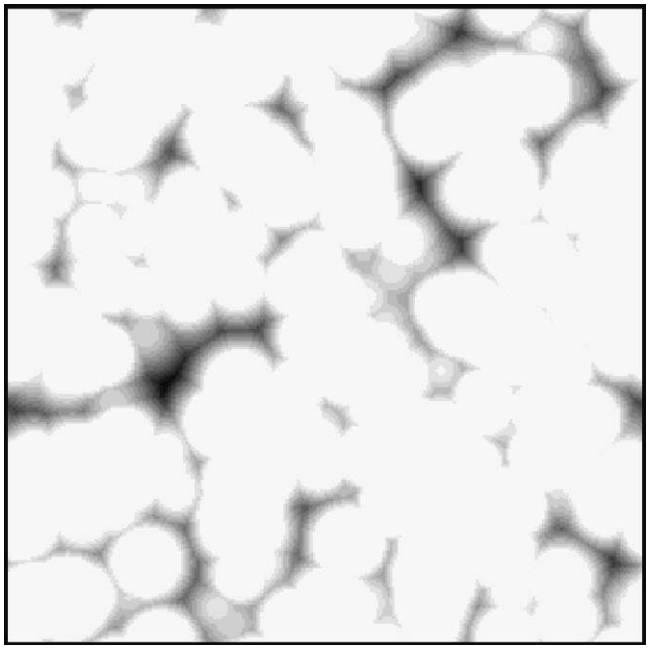

Fig. 3. A two-dimensional cut through the unit cell. Grey: unoccupied volume; white: atoms.

First of all, we applied the Delaunay triangulation to the results of the simulations. Here, the edges of the calculated tetrahedrons were taken as distances between nearest neighbors. The next-nearest neighbors are not taken into account. The triangulation was used to prove, whether the inner structure of the polymer was stable. Fig. 4 shows the distances between the carbon atoms and their nearest neighbors. The upper curve is the sum of all distance distributions. The distributions related to the different partners are shown below. The peaks in the distributions are in good agreement with literature values for bond distances [39] and verify that the simulated polymer inner structure is consistent after the simulation (Fig. 4).

In order to mark the occupied area, the atoms were described first as in Voorintholt et al. as hard spheres with the size of the Van der Waals spheres. The radii taken from the literature [40] are shown in Table 2.

The remaining holes were then scanned by different probe sizes. The tracer radii were varied between 0.03 and 0.17 nm in 0.02 nm steps. The radius of 0.03 nm is smaller than the probes used in earlier studies. Schmitz and Müller-Plathe, for example, only detected holes larger than 63 Å^3 [41]. Further details of our method and tests on various simple systems are described in Ref. [42].

5. Results and discussion

The determined hole size distributions are shown in Fig. 5. These data indicate a linear behavior. A straight line in a double logarithmic plot is consistent to a power law in a linear plot. The exponents of these functions for different tracer radii are shown in Fig. 6. The error bars result from the calculation of these exponents from a simple regression of the logarithmic data. A determination of the generalized shape taken from the ellipsoids of inertia shows that the holes

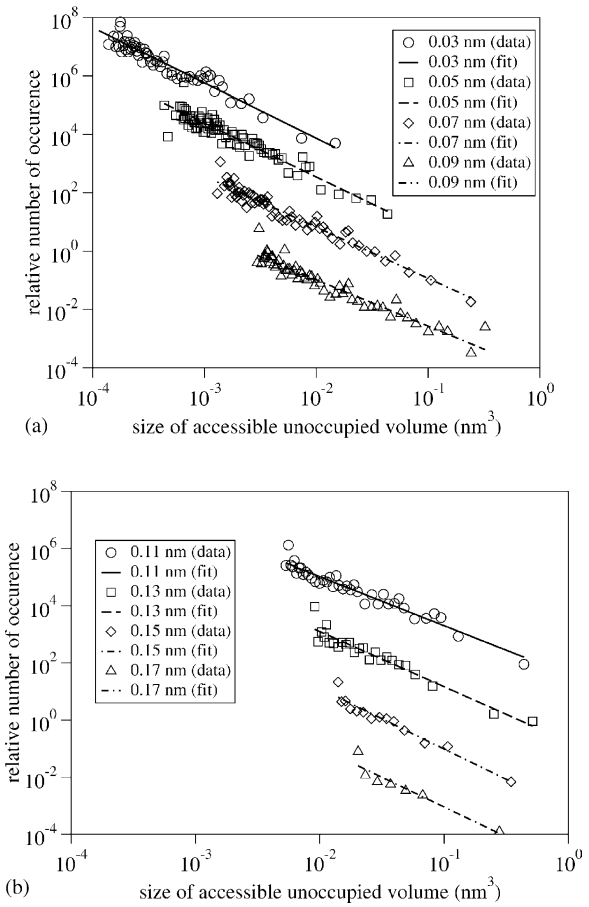

Fig. 5. The hole size distribution determined by scanning the unit cell with different tracer radii. The open symbols show the calculated hole sizes taken from linear regression.

are more elongated than plate like. This is clearly shown in Fig. 7a and b. Presented are the occurrences of the half axis ratios b/a and c/a. Since $a > b > c$, there are no ratios in the rear part of the figure. In Fig. 7a, all holes for the 0.13 nm tracer radius are analyzed for the four simulations. The smallest holes (Fig. 6) are more frequent and they are necessarily spheres. Therefore, there is a peak at $b/a = c/a = 1$. The occurrence along the straight line $b = c$ is a strong indication for a cigar-like elongated shape. To show this more clearly we rescaled the axis for the occurrence in Fig. 7b and cut the top at $b = c = a$. The deviation from the ellipsoid form is described by the parameter D (Eq. (7)). In Fig. 8, we show all detected holes in the PAI unit cells. In this figure, the detected size and the determined D parameters are marked. There is an obvious dependence between D

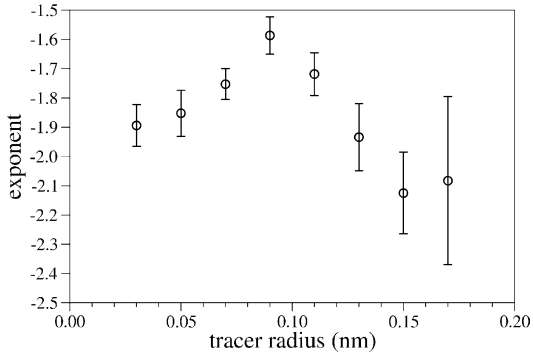

Fig. 6. The exponents of the power law for different tracer radii shown in Fig. 5. The error bars results from the calculation of these exponents for a simple regression of the logarithmic data.

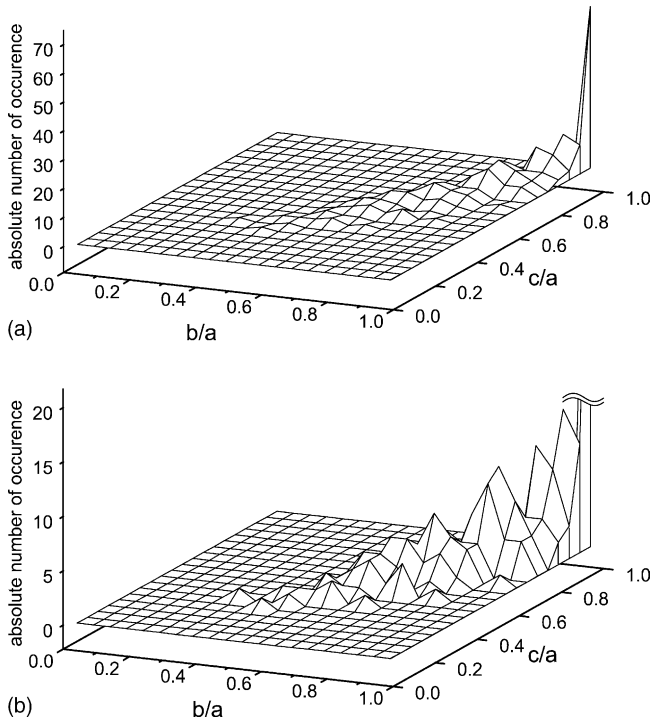

Fig. 7. Representation of the generalized hole shape taken from the ellipsoids of inertia. Presented are the occurrences of the half axis ratios b/a and c/a. Since $a > b > c$, there are no ratios in the rear part of the figure. (a) All holes detected with the tracer radius 0.13 nm in the four simulations. (b) The same figure after rescaling the axis for the occurrence and cutting the top of the peak at $b = c = a$ for sake of clarity.

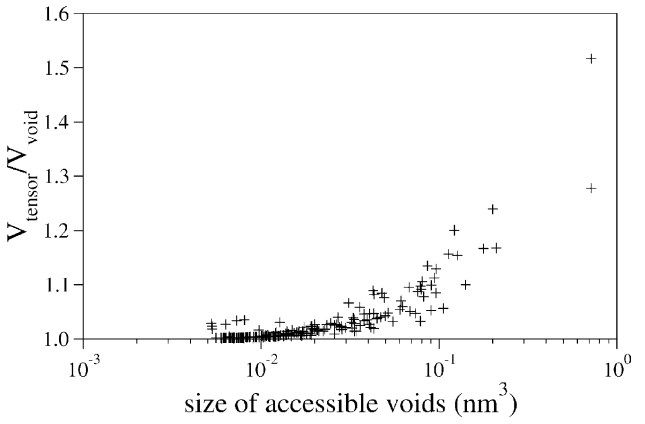

Fig. 8. Deviation from the ellipsoid form described by the parameter D (see Eq. (7)) for all detected holes in the PAI(1) unit cells. There is an obvious dependence between D and the hole size. The larger the hole size the larger is the deviation from the ellipsoid form.

and the hole size. The larger the hole size, the larger is the deviation from the ellipsoid shape. We did not detect hole size distributions with a maximum at intermediate hole sizes as described in Ref. [43].

The average free volume calculated from the PALS data is $0.140 \pm 0.002\,nm^3$ [29]. With a probe radius of 0.13 nm (which is the radius of the positronium) we detected lower "reachable unoccupied volumes" than the average free volume calculated from the PALS data. This behavior was also observed earlier and is explained by the argument that positrons visit several holes during their lifetimes but stay preferentially in the larger holes [33]. An alternative explanation is that the positrons detect the maximum hole size during the free volume fluctuations and therefore "feel the free volume" [27,29].

6. Summary

An improved model to determine the unoccupied volume in an amorphous structure is presented. This model was used to calculate the unoccupied volume of a poly(amid imid) structure from molecular dynamic simulations. Since the reachable unoccupied volume strongly depends on the tracer radius we used different tracer radii to scan the structure. Comparison of the free volume data taken from positron lifetime with the hole sizes calculated from these scans with the radius of the positronium results in smaller values for the holes. This can be explained by the argument that positrons stay preferentially in larger holes or that positrons also detect free volume fluctuations.

Acknowledgements

The authors would like to thank Axel Thran for stimulating discussions and contributions to the computer code. Critical reading of the manuscript by K. Rätzke is gratefully acknowledged.

References

[1] H. Nakanishi, Y.C. Jean, Positronium formation at free-volume in the amorphous regions of semicrystalline PEEK, J. Polym. Sci. B: Polym. Phys. 27 (1989) 1419–1424.
[2] Y.C. Jean, Positron annihilation spectroscopy for chemical analysis: a novel probe for microstructural analysis of polymers, Microchem. J. 42 (1990) 72–102.
[3] S.J. Tao, Positronium annihilation in molecular substances (liquids and solids), J. Chem. Phys. 56 (1972) 5499–5510.
[4] M. Eldrup, D. Lightbody, J.N. Sherwood, The temperature dependence of positron lifetimes in solid pivalic acid, Chem. Phys. 63 (1981) 51–58.
[5] G. Ferrante, Annihilation of positrons from positronium negative ion $e^-e^+e^-$, Phys. Rev. 170 (1968) 76–80.
[6] Z. Yu, J.D. McGervey, A.M. Jamieson, R. Simha, Can positron annihilation lifetime spectroscopy measure the free-volume hole size distribution in amorphous polymers? Macromolecules 28 (1995) 6268–6272.
[7] Y.C. Jean, Comments on the paper can positron annihilation lifetime spectroscopy measure the free-volume hole size distribution in amorphous polymers? Macromolecules 29 (1996) 5756–5757.
[8] W. Triftshäuser, F. Kögel, P. Sperr (Eds.), Positron Annihilation ICPA 12, Material Science Forum, 2000, pp. 343–346.
[9] T. Mukherjee, S.K. Das, B.N. Ganguly, B. Dutta-Roy, Bubble model for positronium annihilation in liquids, Phys. Rev. B 60 (21) (1998) 13363–13366.
[10] D. Gangopadhyay, B.N. Ganguly, T. Makherjee, B. Dutta-Roy, Critical assessment of the bubble model for positronium annihilation in liquids, J. Phys. Condens. Matter 11 (1999) 1463–1471.
[11] D.W. Gidley, W.E. Frieze, T.L. Dull, A.F. Yee, E.T. Ryan, H.-M. Ho, Positronium annihilation in mesoporous thin films, Phys. Rev. B 60 (8) (1999) R5157–R5156.
[12] K. Ciesielski, A.L. Dawidowicz, T. Goworek, B. Jasinska, J. Wawryszczuk, Positronium lifetimes is porous Vycor glass, J. Chem. Phys. Lett. 289 (1998) 41–45.
[13] Y.C. Jean, H. Shi, Positronium lifetime in an ellipsoidal free-volume holes of polymers, J. Non-cryst. Sol. 172 (1994) 806–814.
[14] F. Maurer, ICPA-12: International Conference on Positron Annihilation, Talk 2001.
[15] J.S. Vrentas, C.M. Vrentas, Fickian diffusion in glassy polymer–solvent systems, J. Polym. Sci. B: Polym. Phys. 30 (1992) 1005–1011.
[16] G. Voronoi, Nouvelles applications des paramètres continus à la théorie des formes quadratiques, J. für die reine angewandte Math. 134 (1908) 198–287.
[17] B. Delaunay (B. Delone), Sur la Sphère vide. Bull. l'Academie des Sciences de l'URSS (1934) 793–800.
[18] J.D. Bernal, Geometry of the structure of monatomic liquids, Nature 185 (1960) 68–70.
[19] S. Arizzi, P.H. Mott, U.W. Suter, Space available to small diffusants in polymeric glasses: analysis of unoccupied space and its connectivity, J. Polym. Sci. B: Polym. Phys. 30 (1992) 415–426.
[20] E.J.W. Whittaker, The cavaties in a random close-packed structure, J. Non-crystal. Solids 28 (1978) 293–304.
[21] M. Ahmadzadeh, B. Cantor, Interstitial structure and diffusion in DRP metallic glasses, J. Non-crystal. Solids 43 (1981) 189–219.
[22] B.J. Gellatly, J.L. Finney, Characterisation of models of multicomponent amorphous metals: the radical alternative to the Voronoi Polyhedron, J. Non-crystal. Solids 50 (1982) 313–329.
[23] S. Lee, W.L. Mattice, A "phantom bubble" model for the distribution of free volume in polymers, Comput. Theor. Polym. Sci. 9 (1999) 57–61.
[24] D. Theodorou, U.W. Suter, Shape of unperturbed linear polymers; polypropylene, Macromolecules 18 (1985) 1206–1285.
[25] R. Voorintholt, M.T. Kosters, G. Vegter, G. Vriene, W.G.J. Hol, A very fast program for visualizing protein surfaces, channels and cavities, J. Mol. Graphics 7 (1989) 243–245.
[26] F. Müller-Plathe, L. Laakson, W.F. van Gusteren, Cooperative effects in the transport of small molecules through an amorphous polymer matrix, J. Mol. Graphics 11 (1993) 118–120.
[27] D. Hofmann, L. Fritz, J. Ulbrich, D. Paul, Molecular modelling of amorphous polymer membranes, Polymer 38 (20) (1997) 6145–6155.
[28] C. Nagel, E. Schmidtke, K. Günther-Schade, D. Hofmann, D. Fritsch, T. Strunskus, F. Faupel, Free volume distributions in glassy polymer membranes: comparison between molecular modeling and experiments, Macromolecules 33 (6) (2000) 2242–2248.
[29] C. Nagel, K. Günther-Schade, D. Fritsch, T. Strunskus, F. Faupel, Free volume and transport properties in highly selective polymer membranes, Macromolecules 35 (6) (2002) 2071–2077.
[30] Biosym, 1993. Computational results obtained using software programs from Biosym Technologies of San Diego—molecular mechanics calculations from discover (Version 3.1, 1993) and graphical display using InsightII.
[31] MSI, 1996. Computational results obtained using software programs from Biosym Technologies of San Diego-molecular mechanics

calculations from Discover (Version 4.0.0, 1996) and graphical display using InsightII.
[32] A.T. Hagler, S. Lifson, P. Dauber, J. Am. Chem. Soc. 101 (1979) 5122.
[33] A.T. Hagler, S. Lifson, P. Dauber, J. Am. Chem. Soc. 101 (1979) 5133.
[34] Polymer User Guide, Amorphous Cell Section, Version 4.0.0, Molecular Simulations, San Diego, 1996.
[35] H.J.C. Berendsen, J.P.M. Postma, W.F. van Gunsteren, A. DiNola, J.R. Haak, J. Chem. Phys. 81 (1984) 3684.
[36] A.A. Gusev, U.W. Suter, J. Chem. Phys. 99 (1993) 228.
[37] A.A. Gusev, U.W. Suter, Computer-aided Mater. Des. 1 (1993) 63.
[38] D. Hofmann, L. Fritz, J. Ulbrich, C. Schepers, M. Böhning, Macromol. Theory Simul. 9 (2000) 293.
[39] CRC Handbook of Chemistry and Physics, 62nd ed., CRC Press, Boca Raton, FL, 1981.
[40] D.W. Van Krevelen, Properties of Polymers, third ed., Elsevier, Amsterdam, 1990, p. 72.
[41] H. Schmitz, F. Müller-Plathe, Calculation of the lifetime of positronium in polymers via molecular dynamics simulations, J. Chem. Phys. 112 (2) (1999) 1040–1045.
[42] E. Schmidtke, Ph.D. Thesis, Kiel University, Kiel, 2000.
[43] J. Bohlen, J. Wolff, R. Kirchheim, Determination of free-volume and hole number density in polycarbonates by positron lifetime spectroscopy, Macromolecules 32 (1999) 3766–3773.